International Journal of Mechanical, Industrial and Aerospace Sciences
ISSN: 2517-9950
Vol:2, No:5, 2008

A CFD Study of Sensitive Parameters Effect on the Combustion in a High Velocity Oxygen-Fuel Thermal Spray Gun

S. Hossainpour, and A. R. Binesh

***Abstract*—**High-velocity oxygen fuel (HVOF) thermal spraying uses a combustion process to heat the gas flow and coating material. A computational fluid dynamics (CFD) model has been developed to predict gas dynamic behavior in a HVOF thermal spray gun in which premixed oxygen and propane are burnt in a combustion chamber linked to a parallel-sided nozzle. The CFD analysis is applied to investigate axisymmetric, steady-state, turbulent, compressible, chemically reacting, subsonic and supersonic flow inside and outside the gun. The gas velocity, temperature, pressure and Mach number distributions are presented for various locations inside and outside the gun. The calculated results show that the most sensitive parameters affecting the process are fuel-to-oxygen gas ratio and total gas flow rate. Gas dynamic behavior along the centerline of the gun depends on both total gas flow rate and fuel-to-oxygen gas ratio. The numerical simulations show that the axial gas velocity and Mach number distribution depend on both flow rate and ratio; the highest velocity is achieved at the higher flow rate and most fuel-rich ratio. In addition, the results reported in this paper illustrate that the numerical simulation can be one of the most powerful and beneficial tools for the HVOF system design, optimization and performance analysis.

***Keywords*—**HVOF, CFD, gas dynamics, thermal spray, combustion.

I. Introduction

THE high-velocity oxygen fuel (HVOF) thermal spray is a particulate deposition process in which micro-size particles of metals, alloys or cermets are propelled and heated in a sonic/supersonic combusting gas stream and are deposited on a substrate at high speeds to form a thin layer of lamellar coating. The coatings prepared by HVOF thermal spray process have been widely used in the automotive, aerospace and chemical industries. The HVOF systems employ various kinds of gun nozzle contours, such as convergent-barrel,[1,2] convergent-divergent (or Laval nozzle),[3] convergent-multistage divergent,[4] and convergent-divergent-barrel.[5,6] The HVOF gun systems without any nozzle are also in use.[3].In this study convergent-divergent-barrel system was simulated. In this system during a HVOF thermal spraying as shown in Fig. 1, premixed fuel and oxygen streams are injected into combustion chambers and energy generated by the combustion process is transformed into a hot high-pressure gas.

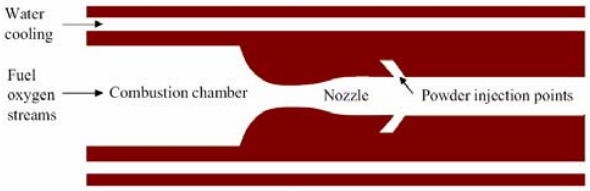

Fig. 1 Schematic of the HVOF thermal spray gun geometry

In order to improve the operation of the HVOF thermal spray process, much experimental work has been done in the last decade to study the effect of operating parameters including gun type, fuel type, feedstock type and size, combustion pressure, fuel/oxygen ratio and spray distance on the particle temperature, velocity, melting ratio, oxidant content and the resulting coating microstructure, porosity, hardness, wear abrasion and corrosion resistance [7-12].

Many parametric studies have been performed on process controlling parameters and coating quality without a detailed understanding of the physical and chemical processes involved, especially in the presence of entrained particles. HVOF spraying involves an intricate interplay between fluid flow, heat transfer, turbulence, chemical reactions, diffusion of multi-component gases, and various gas-particle interactions at elevated temperatures. A detailed understanding of these processes is essential for the HVOF process to reach its full potential. Several previous CFD simulations have investigated gas and particle flows in HVOF thermal spray guns. Power *et al.*[13] and Smith *et al.*[14] modeled a Metco Diamond Jet gun (Sulzer Metco, Westbury, NY) using a steady-state axisymmetric analysis. In the Diamond Jet system, premixed oxygen (O2) and propylene (C3H6) are injected into an air-cooled nozzle. They modeled the internal flow and external flow separately with a finite-rate chemistry model in the internal flow and equilibrium chemistry results as boundary conditions for the external flow. Oberkampf and Talpallikar[15,16] also developed a model of a similar gun geometry, again using an axisymmetric, steady-state analysis. In their work, there was full coupling between the interior and exterior flow fields, and an approximate

S. Hosseinpour is with the Mechanical Engineering Department, Sahand University of Technology, Tabriz, Iran (corresponding author to provide phone: +98-412-3459053; fax: +98-412-3444300; e-mail: hossainpour@sut.ac.ir).

A. R. Binesh is with the Mechanical Engineering Department, Sahand University of Technology, Tabriz, Iran (e-mail: alireza.binesh@yahoo.com).

equilibrium chemistry model was used to treat the combustion of C3H6. Chang and Moore [17] studied the transient flow and temperature distribution in a liquid-fueled HVOF gun. In this gun, oxygen and kerosene are injected into the combustion chamber and gaseous products are accelerated through a converging-diverging throat and along a barrel. They assumed complete combustion of the fuel, allowed for chemical reactions of the gaseous products in the flow through the throat and barrel, but did not simulate the free jet external to the gun. A steady-state solution was found to develop in less than $2\times10^{-3}s$, and, in this system, Mach numbers greater than one were calculated to develop inside the barrel because of the converging- diverging design of the throat of the burner. Because of the inherent complexity of the process, a fundamental understanding of the physicochemical phenomena involved in the HVOF thermal spray process generally requires comprehensive numerical models including computational fluid dynamic (CFD) models [18-22].

In this paper a computational fluid dynamic (CFD) model is developed to predict gas dynamic behavior in a high-velocity oxygen-fuel (HVOF) thermal spray gun in which premixed oxygen and propane are burnt in a combustion chamber linked to a parallel-sided nozzle. The CFD analysis is applied to investigate axisymmetric, steady-state, turbulent, compressible, chemically reacting, subsonic and supersonic flow within the gun. Results describes the general gas dynamic features of HVOF spraying and then gives a detailed discussion of the numerical predictions of a computational fluid dynamic (CFD) analysis. The gas velocity, temperature, pressure and Mach number distributions are presented for various locations inside the convergent-divergent-barrel system.

The specific objectives of the paper are to identify the appropriate governing equations for the Problem, using a computer code to create a computational grid and solve the governing equations on the computational domain, compare the predictions of the numerical simulation and make suggestions for the better performance of the device.

II. Computational Model

A. Model Geometry and the Mesh

The studied HVOF gun is represented schematically in Fig. 1. Fuel and oxygen are injected axially into the combustion chamber, where the fuel burns and the combustion products are accelerated down through the convergent–divergent nozzle and the long parallel-sized barrel. The gun is protected by cooling water to avoid over-heating. Powder particles are injected into the barrel through a tapping angle by a carrier gas in the front of the barrel, this design can effectively reduce the overheating of powder particles. The study is focused on the combustion process and subsequent gas flow pattern, while particle dynamics and gas–particle interaction are not included. With a well designed nozzle configuration, the maximum gas velocity can be up to 2000 m/s, with a Mach number around 2 at the exit of the nozzle.

The computational domain used in the present simulation is shown in Fig. 2. A convergent-divergent nozzle is designed to generate a supersonic jet. Because the gun geometry is symmetrical about its axis, a two-dimensional (2-D) axi-symmetric grid is used to simulate the gas phase flow behavior. The computational grid of this axis-symmetric flow includes the gun and external free jet region as illustrated in Figs. 3 and 4. The grid is finer in the regions where large gradients of flow properties exist, and gradually changes to become coarser in the regions where small gradients of flow properties are expected. This fine mesh size will be able to provide good spatial resolution for the distribution of most variables within the combustion chamber, convergent divergent nozzle, barrel and external domain.

Fig. 2 Computational domain

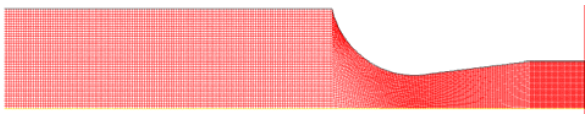

Fig. 3 Grid structure within the combustion chamber and convergent divergent nozzle part

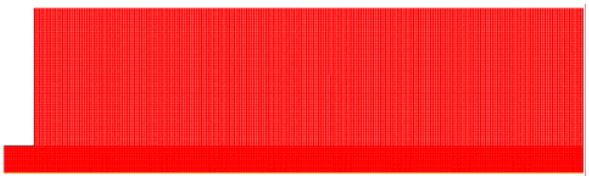

Fig. 4 Grid structure within the External domain

B. Governing Equations

A computer code is used to perform numerical simulations of the fluid flow in HVOF system by solving the conservation equations of mass, momentum, energy and species. A standard, two-equation, realizable $k-\varepsilon$ turbulence model is employed for the turbulent flow field.

Continuity Equation:

$$\frac{\partial \rho}{\partial t}+\frac{\partial}{\partial x_i}(\rho u_i)=0 \tag{1}$$

Momentum Equation:

$$\frac{\partial}{\partial t}(\rho u_i)+\frac{\partial}{\partial x_j}(\rho u_i u_j)=-\frac{\partial p}{\partial x_i}+\frac{\partial \tau_{ij}}{\partial x_j} \tag{2}$$

Where p the static pressure and the stress tensor are τ_{ij} is given by:

$$\tau_{ij}=\mu\left(\frac{\partial u_i}{\partial x_j}+\frac{\partial u_j}{\partial x_i}\right)-\frac{2}{3}\mu\delta_{ij}divV \tag{3}$$

Where μ are the molecular viscosity and the second term on the right hand side is the effect of volume dilation.

Energy Equation:

$$\frac{\partial}{\partial t}(\rho E)+\frac{\partial}{\partial x_i}(u_i(\rho E+p))=\frac{\partial}{\partial x_i}\left(k_{eff}\frac{\partial T}{\partial x_i}-\sum_{j'}h_{j'}J_{j'}+u_j(\tau_{ij})_{eff}\right)+S_h \quad (4)$$

Where k_{eff} is the effective conductivity and J_j is the diffusion flux of species j. The first three terms on the right-hand side of Equation represent energy transfer due to conduction, species diffusion, and viscous dissipation, respectively. S_h includes the heat of chemical reaction, and any other volumetric heat sources we have defined.

In equation (4),

$$E=h-\frac{P}{\rho}+\frac{u_i^2}{2} \quad (5)$$

Where sensible enthalpy h is defined for ideal gases as

$$h=\sum_{j'}m_{j'}h_{j'} \quad (6)$$

Where $m_{j'}$ is the mass fraction of species j and

$$h_{j'}=\int_{T_{ref}}^{T}c_{p,j'}dT \quad (7)$$

Where T_{ref} is 298.15 K.

Species Conservation Equation:

When we choose to solve conservation equations for chemical species, we predicts the local mass fraction of each species, m_i, through the solution of a convection-diffusion equation for the i th species. This conservation equation takes the following general form:

$$\frac{\partial p}{\partial t}(\rho m_{i'})+\frac{\partial}{\partial x_i}(\rho u_i m_{i'})=-\frac{\partial}{\partial x_i}J_{i',i}+R_{i'}+S_{i'} \quad (8)$$

Where R_i is the net rate of production of species i by chemical reaction and S_i is the rate of creation by addition from the dispersed phase. An equation of this form will be solved for $N-1$ species where N is the total number of fluid phase chemical species present in the system. Since the mass fraction of the species must sum to unity, the N th mass fraction is determined as one minus the sum of the $N-1$ solved mass fractions. To minimize numerical error, the N th species should be selected as that species with the overall largest mass fraction, such as N_2 when the oxidizer is air. $J_{i',i}$ is the diffusion flux of species i, which arises due to concentration gradients. We use the dilute approximation, under which the diffusion flux can be written as

$$J_{i',i}=-\rho D_{i',m}\frac{\partial m_{i'}}{\partial x_i} \quad (9)$$

Here $D_{i',m}$ is the diffusion coefficient for species i in the mixture.

The reaction rates that appear as source terms in Equation (8) are computed by eddy dissipation model. The reaction rates are assumed to be controlled by the turbulence instead of the calculation of Arrhenius chemical kinetics. The net rate of production for species i due to reaction r, is given by the smaller of the two expressions below:

$$R_{i,r}=\upsilon'_{i,r}M_{w,i}A\rho\frac{\varepsilon}{k}\min_R\left(\frac{Y_R}{\upsilon'_{R,r}M_{w,R}}\right) \quad (10)$$

$$R_{i,r}=\upsilon'_{i,r}M_{w,i}AB\rho\frac{\varepsilon}{k}\frac{\sum_P Y_P}{\sum_{j'}^{N}\upsilon''_{j,r}M_{w,j}} \quad (11)$$

Where Y_P is the mass fraction of any product species P and Y_R is the mass fraction of a particular reactant R and A,B are empirical constants equal to 4.0 and 0.5.

A wide variety of flow problems can be calculated by using the standard $k-\varepsilon$ model based on the presumption that an analogy between the action of viscous stresses and Reynolds stresses on the mean flow exists. Although it is usually acceptably accurate for simple flows, inaccuracies could rise from the turbulent-viscosity hypothesis and from the equation of turbulence dissipation rate for complex flows. Improvement has been made to the standard $k-\varepsilon$ model; a recent development is the realizable $k-\varepsilon$ model. The transport equations for the realizable $k-\varepsilon$ model are:

Turbulent kinetic transport equation:

$$\frac{\partial}{\partial t}(\rho k)+\frac{\partial}{\partial x_i}(\rho k u_j)=\frac{\partial}{\partial x_i}\left[\left(\mu+\frac{\mu_t}{\sigma_k}\right)\frac{\partial k}{\partial x_j}\right] \quad (12)$$
$$+G_k+G_b-\rho\varepsilon-Y_M+S_k$$

Rate of dissipation of energy from the turbulent flow:

$$\frac{\partial}{\partial t}(\rho\varepsilon)+\frac{\partial}{\partial x_j}(\rho\varepsilon u_j)=\frac{\partial}{\partial x_j}\left[\left(\mu+\frac{\mu_t}{\sigma_\varepsilon}\right)\frac{\partial\varepsilon}{\partial x_j}\right] + \rho C_1 S_\varepsilon - \rho C_2 \frac{\varepsilon^2}{k+\sqrt{\nu\varepsilon}} + C_{1\varepsilon}\frac{\varepsilon}{k}C_{2\varepsilon}G_b + S_\varepsilon \quad (13)$$

Where the turbulent viscosity is

$$\mu_t = \rho C_\mu \frac{k^2}{\varepsilon} \quad (14)$$

The coefficient of dynamic viscosity is

$$C_\mu = \frac{1}{A_0 + A_s(kU/\varepsilon)} \quad (15)$$

In comparison with the standard $k-\varepsilon$ model, the realizable $k-\varepsilon$ model contains a new formulation of the turbulent viscosity where the dynamic viscosity coefficient is no longer constant.

C. Boundary Conditions

A fixed composition (a stoichiometric mixture) of oxygen–propane is specified at the fuel inlet of combustion chamber. The inlet temperature of fuel mixture is considered to be uniform at 300 K. A fixed, uniform mass flow 0.018 kg/s is specified at the inlet. Axi-symmetric boundary conditions are applied along the central axis of the combustion chamber. The interior surfaces of the gun are protected by the cooling water and defined as no-slip wall with a constant temperature of 360Kwhich is the measured temperature for the outflow water. The gas exhausts from the gun to air, where external pressure boundary is applied to the ambient temperature of 300K and atmospheric pressure of $1.013\times10^5\ Pa$.

III. Numerical Model

The numerical method used in this study is a segregated solution algorithm with a finite volume-based technique. The segregated solution is chosen, due to the advantage over the alternative method of strong coupling between the velocities and pressure. This can help to avoid convergence problems and oscillations in pressure and velocity fields. This technique consists of an integration of the governing equations of mass, momentum, species, energy and turbulence on the individual cells within the computational domain to construct algebraic equations for each unknown dependent variable. The pressure and velocity are coupled using the SIMPLE (semi-implicit method for pressure linked equations) algorithm which uses a guess-and-correct procedure for the calculation of pressure on the staggered grid arrangement. It is more economical and stable compared to the other algorithms. The second order upwind scheme is employed for the discretization of the model equations as it is always bounded and provides stability for the pressure-correction equation. The CFD simulation convergence is judged upon the residuals of all governing equations. This "scaled" residual is defined as

$$R^\phi = \frac{\sum_{cells} p\left|\sum_{nb} a_{nb}\phi_{nb} + b - a_p\phi_p\right|}{\sum_{cells} p\left|a_p\phi_p\right|} \quad (16)$$

where ϕ_p is a general variable at a cell p, a_p is the center coefficient, a_{nb} are the influence coefficients for the neighboring cells, and b is the contribution of the constant part of the source term. The results reported in this paper are achieved when the residuals are smaller than 1.0×10^{-4}.

IV. Results

A number of numerical simulations have been performed to study the gas dynamic behavior in a high-velocity oxygen-fuel (HVOF) thermal spray gun in which premixed oxygen and propane are burnt in a combustion chamber linked to a parallel-sided nozzle.

The flow transition from subsonic to supersonic conditions through the convergent–divergent nozzle is vividly shown by the Mach number plot in Fig. 5. The subsonic flow is accelerated in the convergent region, the flow reaches sonic state at the throat and further accelerated to supersonic condition in the divergent region. On entering the barrel, the supersonic flow further expands through a series of shock waves and becomes stabilized.

In this HVOF gun system, key process variables are total gas flow rate, and oxygen-to-fuel gas ratio. Two different total gas flow rates were considered, namely, 21 and 18 g/s , and, at each of these flows, two fuel-to oxygen ratios, namely, 0.25, 0.275, were investigated. In considering differences among simulations, for the range of gas flows and ratios examined, results will be plotted as centerline flow field variable versus axial distance.

Fig. 6 shows the centerline Mach numbers plotted against axial distance. The overall trend is that the Mach number increases sharply as it converges into the nozzle but increases only marginally within the parallel-sided region. A maximum velocity is achieved at the higher total flow (21 g/s) and the higher fuel-to-oxygen ratio (0.3). Conversely, the lower flow (18 g/s) and most oxygen-rich ratio (0.25) give the lowest velocity. Also, the three profiles for a 21 g/s flow rate lie above those for the 18 g/s total flow rate. Fig. 7 shows the variation of centerline gas pressure with axial distance. The pressure remains high within the combustion chamber, decreases sharply in the convergent–divergent nozzle and reaches near atmospheric level in the barrel. It needs to point out that the shocks encountered in the front part of the convergent–divergent nozzle are not desirable which gives rise to energy loss when the thermal energy is converted to kinetic energy in the gas phase. It is possible to design a nozzle with perfect expansion at a particular pressure ratio, however, that will impose a limitation on the operating condition of the nozzle. The combustion chamber dimensions shown in these plot figures are normalized by the corresponding barrel diameter (*D*). . The higher total flow rate

generates significantly higher gas pressures as would be expected, whereas the effect of gas ratio is rather limited.

Fig. 8 shows Contours of gas Mach number outside the HVOF gun and wave structure in supersonic under expanded jet. Because the pressure at the exit of the barrel is lower than the ambient pressure, the jet is over-expanded and adjusts to the ambient pressure by a series of shock diamonds. This pattern of expansion and compression waves is repeated until mixing with the surrounding atmosphere which eventually dissipates the supersonic jet.

Fig. 9 shows the Calculated streamlines of the gas phase outside the HVOF gun. As a result, the gas flows parallel to the substrate near the substrate. This phenomenon is very important since the particles might move radially due to the drag force in the radial direction. To further demonstrate this behavior, we provide the evolution of the axial velocity and radial velocity of the gas in several different locations in the external flow field, as shown in Fig. 10. These locations are based on the distance from the exit of the HVOF torch. It is clearly seen that the axial velocity in the centerline decays along the axial direction, and the jet propagates outwards in the radial direction. Close to the substrate, the axial velocity profile is close to zero while the radial velocity increases far away from the centerline.

V. Summary and Conclusion

This paper describes the gas dynamics features that exist inside and outside a high-velocity oxygen-fuel (HVOF) thermal spray gun in which premixed oxygen and propane are burnt in a combustion chamber linked to a parallel-sided nozzle. Numerical results from the computational fluid dynamics modeling are given and discussed. The gas velocity, temperature, pressure, and Mach number distributions are presented for various locations inside and outside the HVOF system. The two-dimensional numerical simulations show large variations in gas velocity and temperature both inside and outside the torch due to flow features such as mixing layers, shock waves, and expansion waves.

Inside the gun, premixed oxygen and propane burn in the combustion chamber and the hot gas is accelerated along the parallel-sided nozzle. Although the maximum gas temperature reaches 3300 K close to the annular flame front, the centerline temperature only reaches a value of 3000 K. The gas velocity at the end of the nozzle is, 2500 m/s with a Mach number of 2.3. In the free jet region, the calculations predict the existence of shock diamonds. In addition, the results reported in this paper illustrate that the numerical simulation can be one of the most powerful and beneficial tools for the HVOF system design, optimization and performance analysis. The results indicate that the most sensitive parameters that affect the behavior of the system both total gas flow rate and fuel-to-oxygen gas ratio. The axial gas velocity depends on both flow rate and ratio; the highest velocity is achieved at the higher flow rate and most fuel-rich ratio.

References

[1] David L. Mason and Kris Rao: in Thermal Spray Coatings—New Materials, Processes and Applications, F.N. Longo, ed., American Society for Metals, Metals Park, OH, 1984, pp. 51-63.
[2] K.A. Kowaisky, D.R. Marantz, M.F. Smith, and W.L. Oberkampf: in Thermal Spray Research and Applications, T.F. Bernecki, ed., ASM International, Materials Park, OH, 1990, pp. 587-92.
[3] Product Catalogue Diamond Jet, Sulzer Metco (US) Inc., New York, NY, 1995.
[4] Product Catalogue Carbide Jet System (CJS), OZU-Mashinenbau GmbH, Castrop-Rauxel, Germany, 1995.
[5] M.L. Thope and H.J. Richer: in Thermal Spray: International Advances in Coating Technology, C.C. Bernt, ed., ASM International, Materials Park, OH, 1992, pp. 137-47.
[6] G.R. Heath and R.J. Dumola: in Thermal Spray: Meeting the Challenges of the 21st Century, C. Coddet, ed., ASM International, Materials Park, OH, 1998, pp. 1495-1500
[7] de Villiers Lovelock, H.L., Richter, P.W., Benson, J.M., Young, P.M. Parameter study of HP/HVOF deposited WC-Co coatings. Journal of Thermal Spray Technology 7, 1998, 97–107.
[8] Gil, L., Staia, M.H. Influence of HVOF parameters on the corrosion resistance of NiWCrBSi coatings. Thin Solid Films, 2002, 420–421, 446–454.
[9] Hanson, T.C., Settles, G.S. Particle temperature and velocity effects on the porosity and oxidation of an HVOF corrosion-control coating. Journal of Thermal Spray Technology 12, 2003, 403–415.
[10] Khor, K.A., Li, H., Cheang, P.,. Significance of melt-fraction in HVOF sprayed hydroxyapatite particles splats and coatings. Biomaterials 25, 2004, 1177–1186.
[11] Marple, B.R., Voyer, J., Bisson, J.F., Moreau, C. Thermal spraying of nanostructured cermet coatings. Journal of Materials Processing Technology 117, 2001, 418–423.
[12] Zhao, L., Maurer, M., Fischer, F., Lugscheider, E. Study of HVOF spraying of WC–CoCr using on-line particle monitoring. Surface & Coatings Technology 185, 2004, 160–165.
[13] G.D. Power, E.B. Smith, T.J. Barber, and L.M. Chiapetta: "Analysis of a Combustion (HVOF) Spray Deposition Gun," UTRC Report No. 91- 8, UTRC, East Hartford, CT, Mar. 1991.
[14] E.B. Smith, G.D. Power, T.J. Barber, and L.M. Chiapetta: in Application of Computational Fluid Dynamics to the HVOF Thermal Spray Gun,Thermal Spray: International Advances in Coatings Technology,C.C. Berndt, ed., ASM International, Materials Park, OH, 1992, pp. 805- 10.
[15] W.L. Oberkampf and M. Talpallikar: J. Thermal Spray Technol., 1996, vol. 5 (1), pp. 53-61.
[16] W.L. Oberkampf and M. Talpallikar: J. Thermal Spray Technol., 1996, vol. 5 (1), pp. 62-68
[17] C.H. Chang and R.L. Moore: J. Thermal Spray Technol., 1995, vol. 4 (4), pp. 358-66.
[18] Kamnis, S., Gu, S. Numerical modeling of propane combustion in a high velocity oxygen-fuel thermal spray gun. Chemical Engineering and Processing 45, 2006, 246–253
[19] Dolatabadi, A., Mostaghimi, J., Pershin, V. Effect of a cylindrical shroud on particle conditions in high velocity oxy-fuel spray process. Journal of Materials Processing Technology 137, 2003, 214–224.
[20] Li, M., Christofides, P.D.. Multi-scale modeling and analysis of HVOF thermal spray process. Chemical Engineering Science 60, 2005,3649–3669.
[21] Gu, S., Eastwick, C.N., Simmons, K.A., McCartney, D.G. Computational fluid dynamic modeling of gas flow characteristics in a high-velocity oxy-fuel thermal spray system. Journal of Thermal Spray Technology 10, 2001, 461–469.
[22] Mingheng Li, Panagiotis D. Christofides, Computational study of particle in-flight behavior in the HVOF thermal spray process, Chemical Engineering Science 61 ,2006, 6540 – 6552.

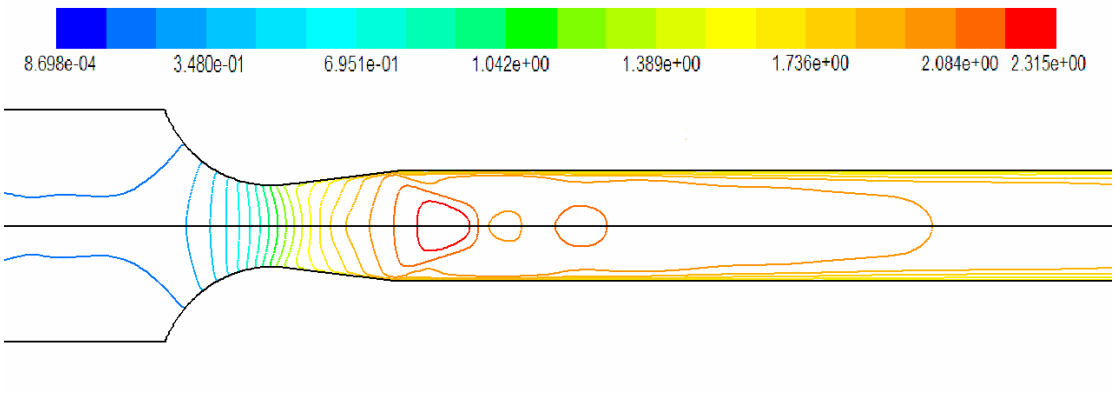

Fig. 5 Predicted March number contours in the convergent–divergent nozzle and barrel

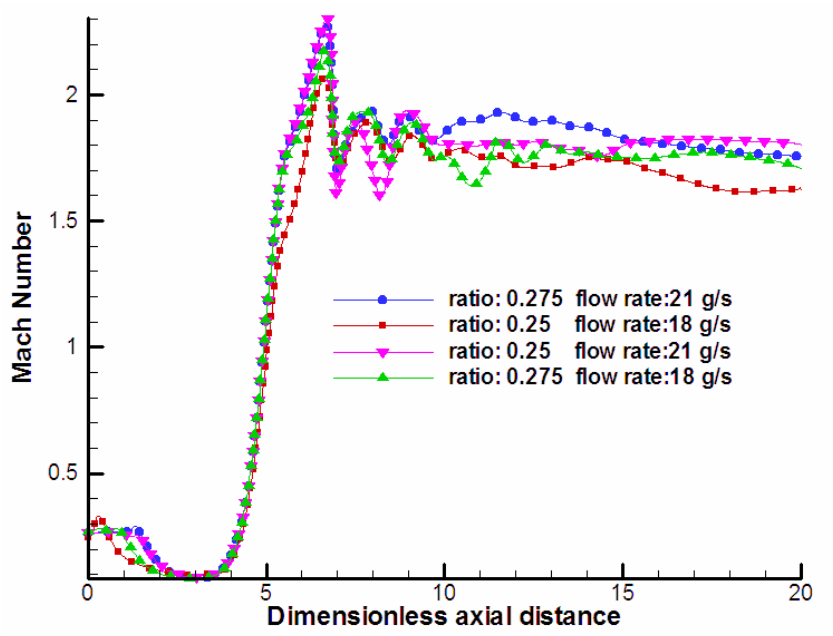

Fig. 6 Variation of Mach number with distance along the centerline (symmetry axis) of the computational domain

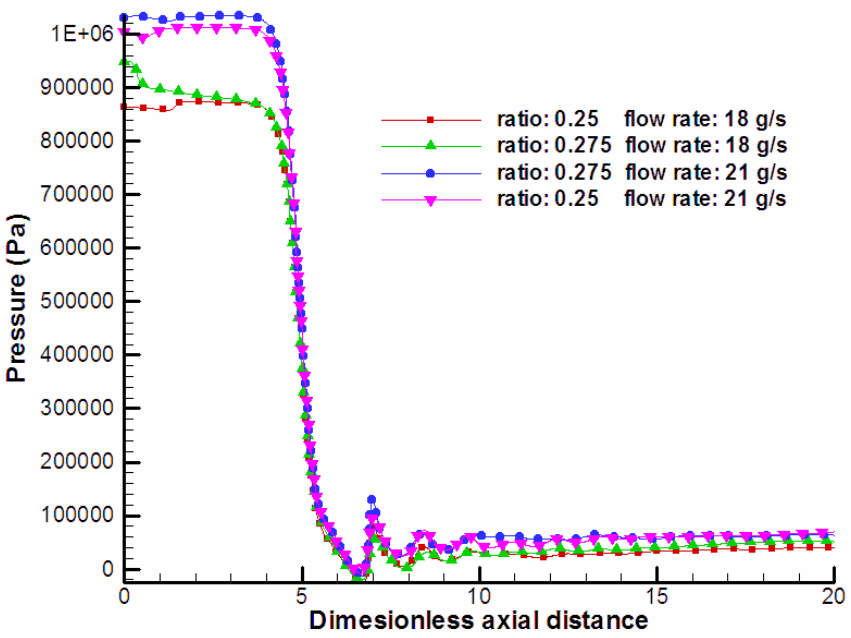

Fig. 7 Variation of pressure with distance along the centerline (symmetry axis) of the computational domain

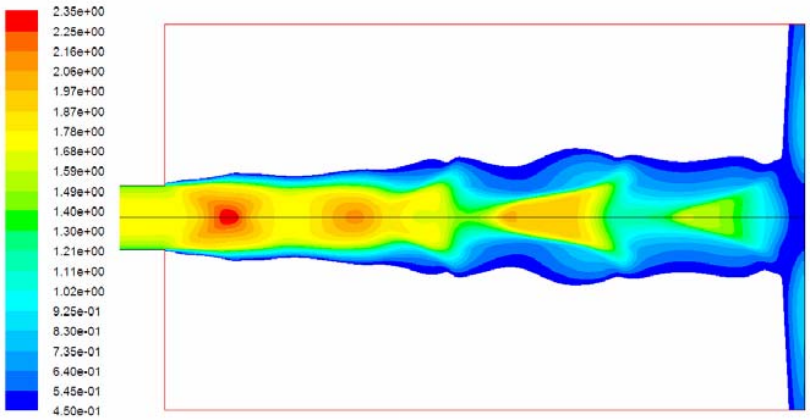

Fig. 8 Contours of gas Mach number outside the HVOF gun and wave structure in supersonic under expanded jet

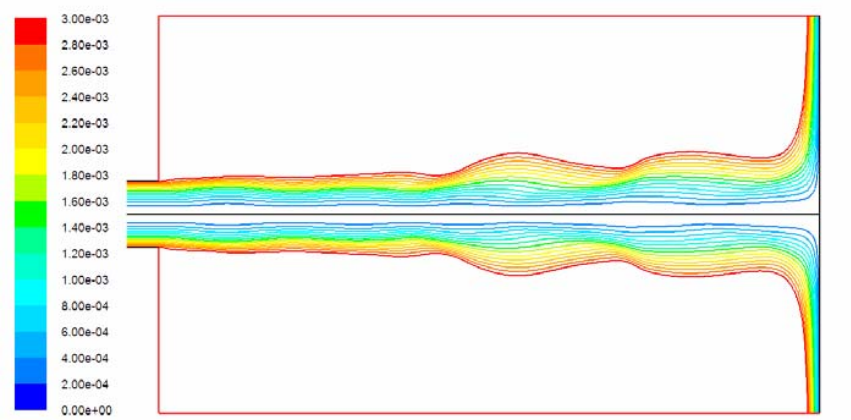

Fig. 9 Calculated streamlines of the gas phase outside the HVOF gun

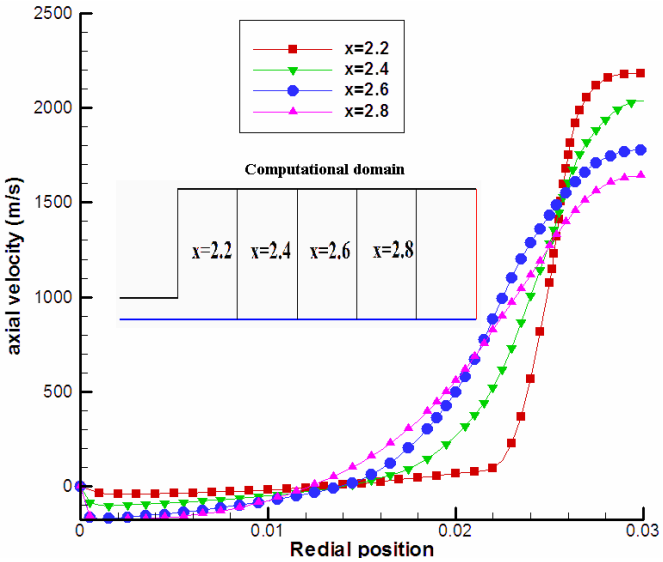

Fig. 10 Axial gas velocity along the radial direction at different axial locations outside the HVOF gun